BBA - Molecular Basis of Disease 1864 (2018) 2010–2020

Contents lists available at ScienceDirect

BBA - Molecular Basis of Disease

journal homepage: www.elsevier.com/locate/bbadis

Age-related NMDA signaling alterations in SOD2 deficient mice

Francisco J. Carvajal[a,b,d], Rodrigo G. Mira[a,b,d], Maximiliano Rovegno[c,d], Alicia N. Minniti[b,d], Waldo Cerpa[a,b,d,*]

[a] Laboratorio de Función y Patología Neuronal, Santiago, Chile
[b] Departamento de Biología Celular y Molecular, Facultad de Ciencias Biológicas, Santiago, Chile
[c] Departamento de Medicina Intensiva, Facultad de Medicina, Santiago, Chile
[d] Pontificia Universidad Católica de Chile, Santiago, Chile

ARTICLE INFO

Keywords:
$SOD2^{+/-}$ mice
Oxidative stress
Synaptic transmission
Hippocampus
NMDARs
Neurodegenerative diseases

ABSTRACT

Oxidative stress affects the survival and function of neurons. Hence, they have a complex and highly regulated machinery to handle oxidative changes. The dysregulation of this antioxidant machinery is associated with a wide range of neurodegenerative conditions. Therefore, we evaluated signaling alterations, synaptic properties and behavioral performance in 2 and 6-month-old heterozygous manganese superoxide dismutase knockout mice ($SOD2^{+/-}$ mice). We found that their low antioxidant capacity generated direct oxidative damage in proteins, lipids, and DNA. However, only 6-month-old heterozygous knockout mice presented behavioral impairments. On the other hand, synaptic plasticity, synaptic strength and NMDA receptor (NMDAR) dependent postsynaptic potentials were decreased in an age-dependent manner. We also analyzed the phosphorylation state of the NMDAR subunit GluN2B. We found that while the levels of GluN2B phosphorylated on tyrosine 1472 (synaptic form) remain unchanged, we detected increased levels of GluN2B phosphorylated on tyrosine 1336 (extrasynaptic form), establishing alterations in the synaptic/extrasynaptic ratio of GluN2B. Additionally, we found increased levels of two phosphatases associated with dephosphorylation of p-1472: striatal-enriched protein tyrosine phosphatase (STEP) and phosphatase and tensin homolog deleted on chromosome Ten (PTEN). Moreover, we found decreased levels of p-CREB, a master transcription factor activated by synaptic stimulation. In summary, we describe mechanisms by which glutamatergic synapses are altered under oxidative stress conditions. Our results uncovered new putative therapeutic targets for conditions where NMDAR downstream signaling is altered. This work also contributes to our understanding of processes such as synapse formation, learning, and memory in neuropathological conditions.

1. Introduction

Oxidative stress is a cellular condition where there is an excess of reactive oxygen species (ROS) and reactive nitrogen species (RNS). ROS include several molecules such as hydrogen peroxide, superoxide and hydroxyl free radicals, which are highly reactive with proteins, membrane lipids and DNA [1,2]. While the generation of ROS is a normal event that occurs in all cells, an imbalance in the equilibrium of the redox status is associated with oxidative stress. The cell maintains redox homeostasis through a complex antioxidant machinery that functions at many levels. For example, the cellular anti-oxidant response includes enzymes such as superoxide dismutase (SOD), glutathione peroxidase, catalase and peroxiredoxins; but also ROS scavengers such as Vitamin E, Vitamin C, β-carotene, uric acid and melatonin [3]. An important member of the antioxidant machinery is the mitochondrial enzyme superoxide dismutase 2 (SOD2), also known as manganese-dependent superoxide dismutase (MnSOD). This protein binds to superoxide, a by-product of oxidative phosphorylation and converts it to hydrogen peroxide or diatomic oxygen [4]. This function allows SOD2 to clear mitochondrial reactive oxygen species (ROS) and, as a result, it confers protection against cell death [5]. Therefore, this enzyme plays an antiapoptotic role counteracting oxidative stress, fibrosis [6], ionizing radiation [7], and inflammatory cytokines [8]. Moreover, the function of SOD2 in the control of ROS levels makes it a relevant element in

Abbreviations: NMDA, *N*-methyl-D-aspartate; ROS, reactive oxidative species; RNS, reactive nitrogen species; SOD, superoxide dismutase; STEP, striatal-enriched protein tyrosine phosphatase; CREB, cAMP response element-binding; AD, Alzheimer's disease; PD, Parkinson's disease; HD, Huntington's disease; AMPA, α-amino-3-hydroxy-5-methyl-4-isoxazolepropionic acid; LTP, long-term potentiation; 4-HNE, 4-hydroxynonenal; 8-OHG, 8-hydroxyguanine; n-Tyr, nitro-tyrosine; MWM, Morris water maze; ACSF, artificial cerebrospinal fluid; fEPSP, field evocated post-synaptic potential; HFS, high-frequency stimulation

* Corresponding author at: Laboratorio de Función y Patología Neuronal, Santiago, Chile.
E-mail address: wcerpa@bio.puc.cl (W. Cerpa).

https://doi.org/10.1016/j.bbadis.2018.03.019
Received 20 October 2017; Received in revised form 19 March 2018; Accepted 20 March 2018
Available online 23 March 2018

aging, cancer, and neurodegenerative diseases [5,9].

Many degenerative illnesses, including Alzheimer's (AD), Parkinson's (PD) and Huntington's (HD) diseases have distinct physiopathological characteristics; however, they share neuropathological hallmarks such as abnormal protein aggregation, increased oxidative stress, mitochondrial dysfunction, and inflammatory processes. These pathologies also share the deregulation of neuronal connections and the disruption of brain circuits. In general, oxidative damage and synaptic failure are early events in the neurodegenerative process [3,10]. Additionally, the age-associated cognitive decline is the consequence of impaired synaptic connectivity and shows a clear relationship with increased oxidative stress [11,12].

In the mammalian brain, excitatory neurotransmission is mainly mediated by glutamate and its ionotropic receptors, AMPA (a-amino-3-hydroxy-5-methyl-4-isoxazolepropionic acid) and *N*-methyl-D-aspartate receptors (NMDARs). Unique properties, including Ca^{2+} permeability, allow NMDARs to play a critical role in brain development, synaptic plasticity and neuropathology [13,14]. NMDARs exist in different forms due to multiple combinations of subunits that can be differentially inhibited by compounds such as zinc or ifenprodil [15,16]. In addition, NMDARs located at synaptic and extrasynaptic sites may constitute two functionally distinct pools that can be activated differentially by several signaling pathways [17]. Synaptic activation of NMDARs induces cell survival signaling. For example, ERK activation via MEK1 [18,19], which induces activation of the master transcription factor CREB by its phosphorylation on serine 133 [20]. On the other hand, extrasynaptic NMDARs stimulation induces shut-off of the CREB pathway through dephosphorylation of its activation site [21]. Also, inactivation of ERK (by extrasynaptic NMDARs stimulation) is associated to Calpain activation and STEP (Striatal-Enriched protein tyrosine phosphatase) cleavage that produces a degradation product of 33 kDa ($STEP_{33}$) [22]. The associated mechanism necessary to maintain the balance between synaptic and extrasynaptic signaling is not clear, but the use of tyrosine phosphatase and kinase inhibitors in hippocampal slices demonstrates a correlation between NMDARs tyrosine phosphorylation and their surface expression [23]. Fyn, an Src family of tyrosine kinases, has several targets among NMDARs subunits. Two very important sites of phosphorylation in the GluN2B subunit are tyrosine 1472, which controls the surface expression of NMDARs [24]; and tyrosine 1336 that is associated with NMDARs enrichment in extrasynaptic membranes [23]. On the other hand, $STEP_{61}$ regulates the dephosphorylated state of the GluN2B subunit through two parallel pathways: by direct dephosphorylation on tyrosine 1472 [25,26], and indirectly via dephosphorylation and inactivation of Fyn [27]. Another phosphatase implicated in the phosphorylated state of NMDARs is PTEN (Phosphatase and tensin homolog deleted on chromosome Ten), initially described as a tumor suppressor with an important regulatory role in the PI3K/Akt signaling pathway [28–30]. Previous work shows that NMDARs-dependent long-term depression (LTD) results in PTEN anchoring to the postsynaptic terminal [31]. This phosphatase has also been associated with other neuropathologies such as AD and Stroke through similar mechanisms dependent on NMDARs phosphorylated status [32,33].

In this work, we used 2 and 6-month-old heterozygous knockout mice with an alteration in their antioxidant system ($SOD2^{+/-}$: low activity of SOD2) and normal *wild-type* (WT) mice to assess their behavioral performance and synaptic transmission under oxidative stress conditions, focusing our attention in the downstream signaling of NMDARs activation. We show that imbalance in the production of ROS causes oxidative damage in proteins, membrane lipids, and DNA in several brain structures, including the hippocampus and cortex. ROS damage also correlates with age. Furthermore, we found impairments in the processes of learning and memory, and alterations in glutamatergic synaptic transmission, mainly in the NMDARs response. We found increased extrasynaptic NMDARs signaling and changes in the molecular machinery implicated in the distribution of these receptors. Our results show increased levels of STEP and PTEN, two phosphatases that lower the synaptic form of NMDA receptors; and also decreased levels of serine-133-phosphorylated CREB, a master transcriptional factor activated by the synaptic response. Using a heterozygous knockout mouse model, we provide a mechanistic understanding of the signaling pathways compromised by high levels of ROS. We show that oxidative stress results in alterations in NMDARs, including the imbalance between synaptic and extrasynaptic signaling. These changes caused by ROS have consequences in brain function, possibly by controlling NMDARs trafficking and destination to the plasma membrane.

Table 1
List of antibodies used for western-blot analysis and immunofluorescence studies. The specificity, isotype, clone number and commercial source of the antibodies used throughout the study are indicated. All antibodies were used according to the manufacturer's instructions, indicating the dilution and technique used for the antibodies.

Antibody	Company	Dilution
4-4-Hydroxynonenal (4-HNE)	USBiological	1:200 for immunofluorescence; 1:1000 for Western-blot
8-Hydroxyguanine (8-OHG)	Santa Cruz Biotechnology	1:200 for immunofluorescence
Nitrotyrosine (n-Tyr)	USBiological	1:200 for immunofluorescence
CREB (phosphor-S133) clone 10E9 (p-CREB)	AbCAM	1:200 for immunofluorescence and 1:2000 for Western blot
STEP clone 23E5	Novus Biological	1:200 for immunofluorescence and 1:1000 for Western blot
Phospho-NMDAR2B (Tyr1336) (p-1336)	Thermofisher Scientific	1:2000 for Western-blot analysis
PTEN	R&D Systems	1:1000 for Western-blot
Phospho-NMDAR2B (Tyr1472) (p-1472)	Cell Siganlinf Technology	1:1000 for Western-blot
NMDAR2B	Invitrogen	1:1000 for Western-blot
GADPH	Santa Cruz Biotechnology	1:1000 for Western-blot
Actin	Novus Biological	1:1000 for Western-blot
Tubulin	Santa Cruz Biotechnology	1:1000 for Western-blot

2. Experimental procedures

2.1. Chemicals and antibodies

The primary antibodies used are listed in Table 1. All secondary antibodies used were obtained from Jackson 2.2.-Immunoresearch, (dilution 1:200; Baltimore, USA). Chemicals used: 2,3-Dioxo-6-nitro-1,2,3,4-tetrahydrobenzo[*f*]quinoxaline-7-sulfonamide disodium salt (NBQX, Tocris, Bristol, UK), Picrotoxin (PTX, Tocris, Bristol, UK), (5*S*,10*R*)-(+)-5-Methyl-10,11-dihydro-5H-dibenzo[*a*,*d*]cyclohepten-5,10-imine maleate (MK-801, Tocris, Bristol, UK).

2.2. Animals

Heterozygous $Sod2^{tm1Leb}$/J mice ($SOD2^{+/-}$; breeding pairs), congenic in the C57BL/6J background, were originally obtained from The Jackson Laboratory (Sacramento, CA, USA). A breeding colony was established by crossing $SOD2^{+/-}$ with wild-type mice. The littermates were genotyped before weaning as described in the genotyping protocols database from Jax Labs. Mice were fed ad libitum. Animals were housed at the Animal Facility of the Facultad de Ciencias Biológicas, Pontificia Universidad Católica de Chile.

2.3. Slice preparation and electrophysiology

Transverse slices (400 μm) from the dorsal hippocampus were cut under cold artificial cerebrospinal fluid (ACSF, in mM: 124 NaCl, 2.6 $NaHCO_3$, 10 D-glucose, 2.69 KCl, 1.25 KH_2PO_4 2.5 $CaCl_2$, 1.3 $MgSO_4$, y 2.60 $NaHPO_4$) using a Vibratome (BSK microslicer DTK-1500E, Ted Pella, Redding, CA, USA) and incubated in ACSF for 1 h, at room

temperature. In all experiments, 10 μM PTX was added to suppress inhibitory GABAA transmission. Slices were transferred to an experimental chamber (2 ml), superfused (3 ml/min, at room temperature) with gassed ACSF (using 95% O_2/5% CO_2), and visualized by transillumination with a binocular microscope (Amscope, Irvine, CA, USA). To evoke field excitatory postsynaptic potentials (fEPSPs), we stimulated with bipolar concentric electrodes (Tungsten, 125 μm OD diameter, Microprobes) connected to an isolation unit (Isoflex, AMPI, Jerusalem, Israel). The stimulation was performed in the Stratum Radiatum within 100–200 μm from the recording site. Recordings were filtered at 2.0–3.0 kHz, sampled at 4.0 kHz using an A/D converter (National Instrument, Austin, TX, USA), and stored with the WinLTP program [34,35]. The basal excitatory synaptic transmission was measured using an input/output curve protocol, which consisted of eight stimuli ranging from 200 to 900 μA (the interval between stimuli was 10 s). To generate LTP, we used high-frequency stimulation (HFS) protocol, which consisted of 2 trains at 100 Hz of stimuli with an intertrain interval of 10 s. Data were collected and analyzed offline with pClamp 10 (Molecular Devices, San Jose, CA, USA).

2.4. Behavioral tests: classical model test

The Morris water maze (MWM) task was performed as described below [36,37]. Briefly, male mice were trained in a 1.1 m diameter circular pool (opaque water, 50 cm deep) filled with 19–21 °C water. A submerged 9-cm platform (1 cm below the surface, invisible to the animal) was used for training, with maximum trial duration of 60 s and 10 s on the platform at the end of the trials. Each animal was trained to locate the platform. The test was performed with three trials per day, and swimming was monitored using an automatic tracking system (ANY-maze video tracking software, Stoelting Co, Wood Dale, IL, USA). This system was used to measure the latency time (in seconds) required for the animal to reach the platform and the time spent in each quadrant (in seconds). After testing, the mouse was gently removed from the maze and returned to its cage.

2.5. Memory flexibility test

The MWM was performed as described below [38]. Briefly, mice were trained in a 1.1 m diameter circular water maze (opaque water, 50 cm deep, 19–21 °C, with a 9-cm platform 1 cm below the surface, a maximum trial duration of 60 s, 10 s on the platform at the end of the trials and a delay time between 10 and 15 min). Each animal was trained for one pseudo-random location of the platform per day for 4 days, with a new platform location each day. Up to 10 training trials were performed per day until the criterion of 3 successive trials with an escape latency of < 20 s was met. Upon testing completion, the mouse was gently removed from the maze and returned to its cage. The animals were tested for the next location on the following day. Data were collected using a water maze video tracking system (ANY-maze video tracking software, Stoelting Co, Wood Dale, IL, USA).

2.6. Immunoblotting

The hippocampi and cortices of treated or control heterozygous knockout mice were dissected on ice and immediately processed as previously described [39,40]. Briefly, hippocampal and cortical tissues were homogenized in RIPA buffer (10 mM Tris-Cl, pH 7.4, EDTA 5 mM, 1% NP-40, 1% sodium deoxycholate, and 1% SDS) supplemented with a protease inhibitor mixture (25 mM NaF, 100 mM Na_3VO_4 and 30 μM $Na_4P_20_7$) using a Potter homogenizer and then passed sequentially through different caliber syringes. Protein samples were centrifuged twice at 14,000 rpm at 4 °C for 15 min. Protein concentration was determined using a BCA protein assay kit (Pierce, Thermo Fisher Scientific, Waltham, MA, USA). Samples were resolved by SDS-PAGE, followed by immunoblotting on PVDF membranes. Western blot assays were performed as previously described [40].

2.7. Immunohistochemical procedures

Perfusion, fixation and free-floating immunofluorescence procedures were performed as previously described [39]. Washes and immune reagent dilutions were performed using 0.01 M PBS with 0.2% Triton X-100 (PBS-T) in all immunohistochemical experiments, with two PBS-T washes per antibody incubation. After PBS and PBS-T washes, 30 μm thick brain slices were used for the detection of STEP, n-Tyr, 8-OHG, and 4-HNE. For p-CREB detection 10 μm thick slices were incubated in 0.15 M Glycine and 10 mg/ml $NaBH_4$ to decrease background auto-fluorescence. Slices were washed again with PBS and PBS-T and blocked with 3% BSA for 1.5 h, at room temperature to avoid non-specific binding. Detection of all targets of interest was performed using primary antibodies incubated overnight in PBS-T containing 0.5% BSA at 4 °C. After washing with PBS-T, sections were incubated for 2 h at room temperature with the respective secondary antibody in PBS-T containing 0.5% BSA. Then, sections were washed with PBS-T, PBS, and water, mounted on gelatin-coated slides and cover slipped with fluorescence mounting medium.

To detect morphological changes in the hippocampus, the slices were dewaxed to water and subjected to Nissl staining. Before staining, all sections were mounted on gelatin-coated slides, air-dried, stained using 0.1% cresyl violet acetate and cover slipped with Canada balsam.

2.8. Image analysis

Stained brain sections were photographed using an Olympus BX51 microscope coupled with a Micro-publisher 3.3 RTV camera (QImaging, Surrey, BC, Canada). The luminance of the incident light and the time of exposure were calibrated to assign pixel values ranging from 0 to 255 in RGB image (no-light to full-light transmission) and were used on all preparations. The images were loaded onto ImageJ v.1.40 g software (NIH) for analysis. Selection of areas for measurement was performed by manual threshold adjustment or by direct manual selection of ROIs in heterogeneous stains.

2.9. Statistical analysis

Results are expressed as mean ± standard error. Data were analyzed using one-way ANOVA, followed by Bonferroni's post hoc test. A p-value ≤ 0.05 was considered as statistically significant. Statistical analysis was performed using the Prism software (GraphPad Software Inc.).

3. Results

3.1. Oxidative stress markers are increased in hippocampal slices from $SOD2^{+/-}$ animals

The heterozygous $SOD2^{+/-}$ mice used in this study exhibit decreased SOD2 activity in several tissues [41]. SOD2 activity in the brain of 5-week-old $SOD2^{+/-}$ animals is at least 79% lower than in WT mice of the same age [41]. We focused mainly on the CA3 and CA1 areas of the hippocampus because of their essential participation in learning and memory [42]. All electrophysiological recordings were made in these areas.

The decrease of the antioxidant barrier provided by SOD2 triggered a marked increase in oxidative stress markers. This increment becomes more pronounced as the animals age. We evaluated three oxidative stress markers by immunofluorescence: nitro-tyrosine (n-Tyr; Fig. 1A), 4-hydroxynonenal (4-HNE; Fig. 1B) and 8-hydroxiguanine (8-OHG; Fig. 1C) in the CA1 and CA3 regions in hippocampal slices from wild-type (WT) and $SOD2^{+/-}$ mice of two different ages (2- and 6-month-old). n-Tyr, a product of tyrosine nitration mediated by reactive

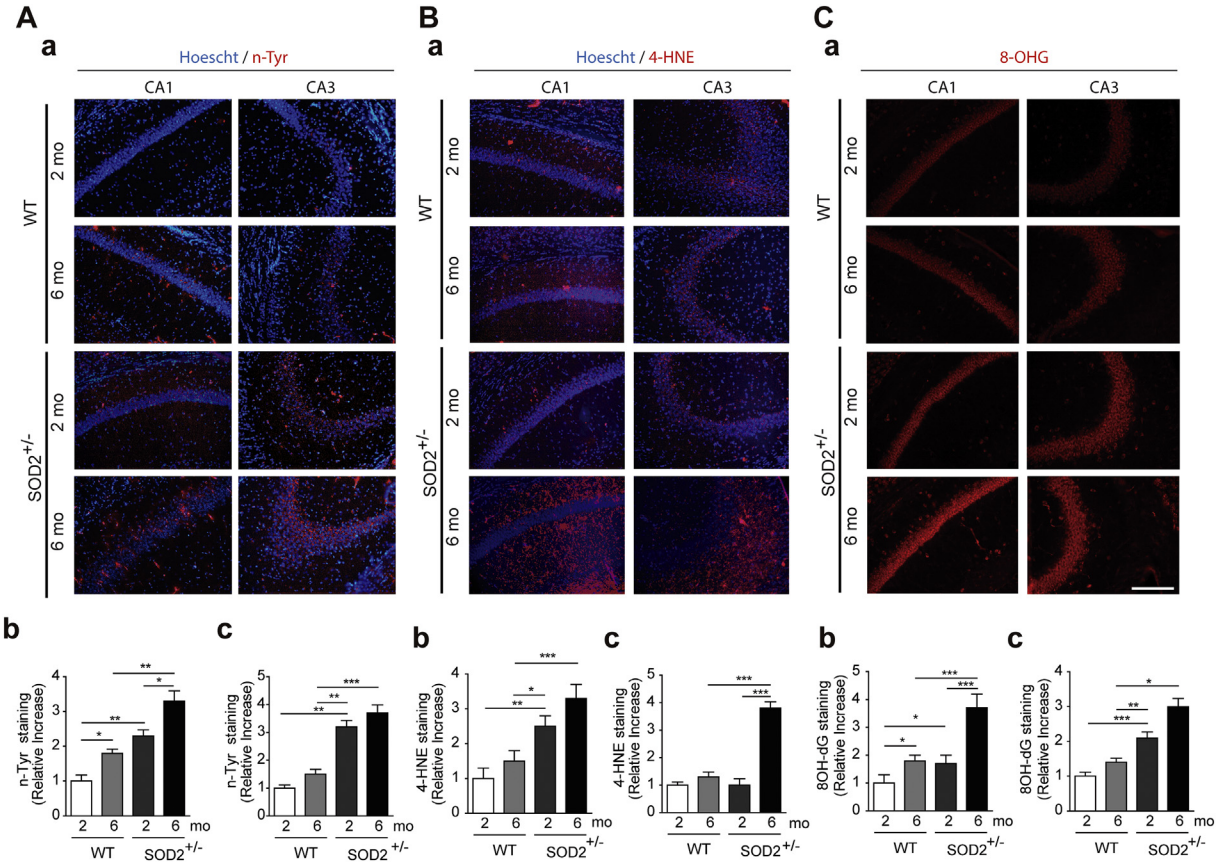

Fig. 1. Oxidative stress markers are increased in hippocampal slices from SOD2$^{+/-}$ mice. Aa. Representative immunofluorescence images showing n-Tyr in hippocampal slices from 2 and 6-month-old WT and SOD2$^{+/-}$ mice. The graphs show the quantification of fluorescence intensity in the CA1 (Ab) and CA3 regions (Ac). Ba. Representative immunofluorescence images showing 4-HNE in hippocampal slices from 2 and 6-month-old WT and SOD2$^{+/-}$ mice. The graphs show the quantification of fluorescence intensity in the CA1 (Bb) and CA3 regions (Bc). Ca. Representative immunofluorescence images showing 8-OHG in hippocampal slices from 2 and 6-month-old WT and SOD2$^{+/-}$ mice. The graphs show the quantification of fluorescence intensity in the CA1 (Cb) and CA3 regions (Cc). Bar = 100 μm. Three animals were used per experimental group. Data are means ± S.E. Statistical differences were calculated by ANOVA, followed by post hoc Bonferroni's test. Asterisks indicate statistical significance of the observed differences (*$p < 0.05$; **$p < 0.01$; ***$p < 0.001$).

nitrogen species such as peroxynitrite anions and nitrogen dioxide, increases significantly in the CA1 region of WT mice as they get older (Fig. 1Aa and Ab). n-Tyr staining in 2-month-old SOD2$^{+/-}$ mice is similar to what we observe in 6-month-old WT mice (Fig. 1Aa, Ab). Moreover, n-Tyr staining in 6-month-old SOD2$^{+/-}$ mice is significantly increased compared to 6-month-old WT mice (Fig. 1Aa and 1Ab). In the CA3 region, no significant differences in n-Tyr were observed between 2 and 6-month-old WT mice (Fig. 1Aa and Ac). On the other hand, the levels of n-Tyr in 2-month-old SOD2$^{+/-}$ mice are higher than in 2- and 6-month-old WT animals. n-Tyr staining in the CA3 region increases significantly in SOD2$^{+/-}$ mice as they get older (Fig. 1Aa and Ac).

We also evaluated the oxidative stress marker 4-HNE, an aldehyde product of lipid peroxidation. 4-HNE has been implicated in the etiology of pathological changes triggered by oxidative stress and it seems to be a key mediator of oxidative-stress-induced cell death through a mitochondria-dependent pathway involving cytochrome-c release and caspase-3 activation [43]. We did not find significant differences in 4-HNE levels in the CA1 and CA3 regions of the hippocampus from 2 and 6-month-old WT mice (Fig. 1Ba, b, and c). However, we observed a two-fold increase in 4-HNE immunostaining in the CA1 region form 2-month-old SOD2$^{+/-}$ animals compared to WT mice of the same age; and an increase of over three-fold in 6-month-old SOD2$^{+/-}$ mice (Fig. 1Ba and 1Bb). In the CA3 region, we only observed increased 4-HNE levels in 6-month-old SOD2$^{+/-}$ mice (Fig. 1Ba and 1Bc).

Finally, we analyzed 8-OHG, the most common DNA lesion resulting from elevated reactive oxygen species, in the hippocampus of WT and SOD2$^{+/-}$ mice. We found a two-fold increase in 8-OHG in the CA1 region from 6-month-old WT and 2-month-old SOD2$^{+/-}$ mice when compared to 2-month-old WT animals. Moreover, 6-month-old SOD2$^{+/-}$ mice showed a marked increase of 8-OHG in this area (Fig. 1Ca and 1Cb). We did not find significant differences in the CA3 area from 2 and 6-month-old WT animals (Fig. 1Ca and 1Cc). 8-OHG increased two-fold in 2-month-old SOD2$^{+/-}$ mice compared to 2-month-old WT animals, whereas 6-month-old SOD2$^{+/-}$ mice showed increased 8-OHG levels of over two-fold compared to 6-month-old WT animals (Fig. 1Ca and 1Cc).

Similar results have been reported for 4-HNE and 8-OHG in a model of traumatic brain injury [44] in which oxidative stress is part of the damage mechanism. In conclusion, decreased levels of the antioxidant enzyme SOD2 significantly increased the oxidative stress markers n-Tyr, 4-HNE and 8-OHG in the mouse hippocampus. Other brain structures such as the cortex and the hypothalamus show similar increments in oxidative stress markers (Supplementary Fig. 1).

3.2. SOD2$^{+/-}$ mice show spatial memory impairments that intensify with age

Oxidative damage and cognitive deficits are common features of several neuropathological conditions including AD, PD, and HD [2,3,39,45,46]. Therefore, we decided to evaluate the cognitive performance of SOD2$^{+/-}$ mice, which have high levels of oxidative stress markers in the hippocampus (Fig. 1). The hippocampal function was

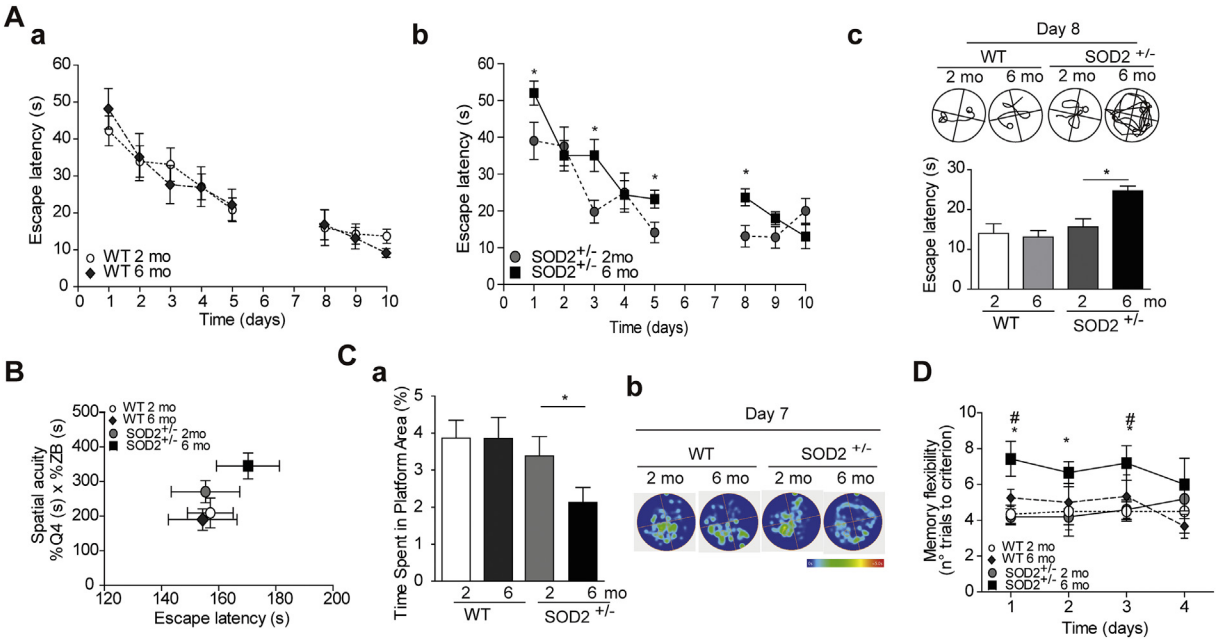

Fig. 2. SOD2$^{+/-}$ mice show spatial memory impairments that intensify with age. Behavioral performance was tested using the standard MWM test. Aa. Escape latency (time to reach the hidden platform) of 2 and 6-month-old WT mice. Ab. Escape latency of 2 and 6-month-old SOD2$^{+/-}$ mice. Ac. Representative swimming trajectories and escape latency for WT and SOD2$^{+/-}$ mice of different ages on day 8. B. Spatial acuity for 2 and 6-month-old WT and SOD2$^{+/-}$ mice after 2 weeks of training. Ca. Analysis of the time mice spent swimming in the area near the platform when it was removed on day 11. Cb. Representative heat map of time spent in the platform area on day 11. D. Behavioral performance of 2 and 6-month-old WT and SOD2$^{+/-}$ mice in the memory flexibility test. Six animals were used per experimental group. Data are means ± S.E. Statistical differences were calculated by ANOVA, followed by post hoc Bonferroni's test. Asterisks indicate statistical significance of the observed differences (*$p < 0.05$, between 6-month-old WT and SOD2$^{+/-}$ mice, #$p < 0.05$ between 2 and 6-month-old SOD2$^{+/-}$ mice). Curves were analyzed by Repeated Measures ANOVA.

tested using the Morris water maze spatial memory test. For this task, mice are required to learn the location of a hidden platform based on external cues [37]. No significant differences were observed between 2 and 6-month-old WT mice during the time of testing (Fig. 2Aa). However, 6-month-old SOD2$^{+/-}$ mice showed a significant increase in escape latency at several time points during the test when compared with 2-month-old SOD$^{+/-}$ (Fig. 2Ab) and same age WT mice. This increase in escape latency was clearly observed on day 8. The representative swimming paths are shown in Fig. 2Ac (top). 6-month-old SOD2$^{+/-}$ mice swim in circles around the pool while 2 and 6-month-old WT mice and 2-month-old SOD2$^{+/-}$ mice swim near the platform. This observation was confirmed when we compared escape latency between 2 and 6-month-old SOD2$^{+/-}$ mice (Fig. 2Ac, bottom). Fig. 2B shows the relationship between spatial acuity and the average escape latency of animals from the different experimental groups. The graph shows that 6-month-old SOD2$^{+/-}$ mice are located in a region of the graph that corresponds to high-escape latency values and low-spatial acuity scores. In contrast, 2-month-old SOD2$^{+/-}$ mice and 2 and 6-month-old WT mice show low-escape latency values and low spatial acuity scores (Fig. 2B).

On day 11 of the memory task, the platform was removed in a probe test that measures the time mice spend swimming in the former area, near the initial platform location (a circular area with twice the platform radius). 2 and 6-month-old WT mice and 2-month-old SOD2$^{+/-}$ mice spend more time in the platform area than 6-month-old SOD2$^{+/-}$ mice. This observation was confirmed when we compared escape latency between 2 and 6-month-old SOD2$^{+/-}$ mice (Fig. 2Ca and b), demonstrating the inability of 6-month-old SOD2$^{+/-}$ mice to remember the platform location. Additionally, we evaluated the animals' cognitive performance using a modified spatial memory paradigm associated with episodic memory (memory flexibility) that has been shown to be more sensitive in detecting hippocampal dysfunction. The analysis of behavioral performance indicates that, in the 3 first days, 6-month-old SOD2$^{+/-}$ mice required more trials to achieve the learning criterion (see Experimental procedures) than 2-month-old animals of the same genotype and 6-month-old WT mice (Fig. 2D). Additionally, we measured the swimming speed of experimental groups in order to detect possible motor problems. However, we did not observe significant differences between the groups (Supplementary Fig. 2). Altogether, the results indicate that lowering the antioxidant barrier by eliminating one copy of the SOD2 gene is not sufficient to produce cognitive failure in 2-month-old animals. However, the accumulation of oxidative stress species in 6-month-old SOD2$^{+/-}$ mice compromises hippocampal-dependent behavioral performance.

3.3. SOD2$^{+/-}$ mice show alterations in the hippocampal structure and synaptic failure that correlate with age

Nissl body staining is a marker for mature neurons and can be used to detect neuronal loss and apoptosis [47]. Nissl analysis showed neuropathological changes in the CA1 and CA3 regions of the hippocampus in 6-month-old SOD2$^{+/-}$ mice, including neuronal loss and shrinkage or disappearance of nuclei (Fig. 3A). These features are absent in 2-month-old SOD2$^{+/-}$ mice and in 2 and 6-month-old WT mice. Furthermore, the number of Nissl bodies significantly decreased in the CA1 and CA3 regions of the hippocampus of 6-month-old SOD2$^{+/-}$ mice compared to 2 and 6-month-old WT mice and to 2-month-old SOD2$^{+/-}$ mice (Fig. 3Aa and b).

In order to evaluate the effect of decreased SOD2 activity and oxidative stress accumulation on synaptic transmission at different ages, we recorded synaptic activity in Schaffer collateral-CA1 synapses evoking field excitatory postsynaptic potential. We performed input-output experiments to test synaptic strength. We analyzed input-output curves for total synaptic response and input-output curves for NMDARs response using 20 μM NBQX, an AMPAR inhibitor (Fig. 3Ba and 3Bb, respectively). We did not find significant differences in total currents or in NMDARs dependent currents between 2 and 6-month-old WT animals (Fig. 3Baand Bb). However, we found a significant decrease in

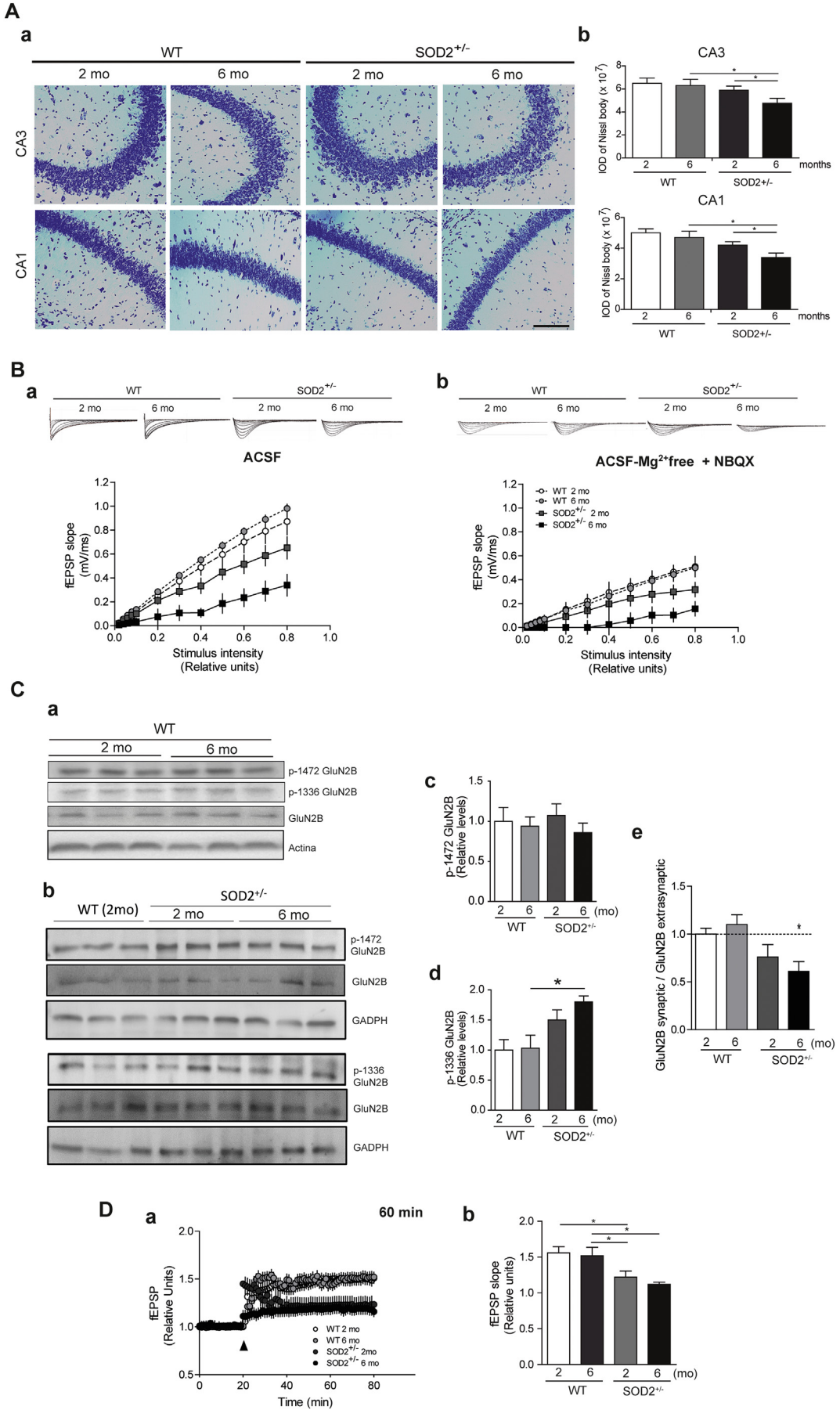

(caption on next page)

Fig. 3. SOD2$^{+/-}$ mice show alterations in the hippocampal structure and synaptic failure that correlate with age. **Aa.** Representative Nissl staining images showing Nissl bodies in the hippocampi of WT and SOD2$^{+/-}$ mice. Top: CA1, bottom: CA3. Ab. Quantification of Nissl bodies in the CA1 (top graph) and CA3 (bottom graph) regions of the hippocampi of WT and SOD2$^{+/-}$ mice of different ages. IOD: integrated optical density in CA1 and CA3 hippocampal areas. **Ba.** fEPSP slope induced by the input-output protocol to record total responses or responses corresponding to NMDARs (Bb) from 2 and 6-month-old WT and SOD2$^{+/-}$ mice. **C.** Immunoblot analyses of phosphorylated GluN2B subunits of NMDARs and densitometric analysis of tyrosine 1472 and tyrosine 1336 phosphorylation in hippocampi lysates from 2 and 6-month-old (Ca). WT mice and 2 and 6-month-old SOD2$^{+/-}$ mice (Cb). Densitometric analysis of phospho-tyrosine 1472 (Cc), phospho-tyrosine 1336 (Cd) in hippocampal lysates from WT and SOD2+/− mice. Normalized ratio of phospho-tyrosine 1472 (synaptic) and phospho-tyrosine 1336 (extrasynaptic) GluN2B subunit (Ce) Da. LTP was generated by HFS in the hippocampal CA1 area in slices from 2 and 6-month-old WT and SOD$^{+/-}$ mice. Quantification of fEPSP slope 60 min after HFS in hippocampal slices from SOD$^{+/-}$ and WT mice of different ages (Db). Bar = 100 μm. The dots and bars represent the mean ± SE from 9 different slices. Three animals were used per experimental group for electrophysiological experiments and six animals for biochemical analyses. Asterisks indicate statistical significance of the observed differences (*$p < 0.05$). Data are presented as means ± S.E.M. Statistically significant differences were calculated by one-way ANOVA, followed by Bonferroni's post hoc test.

total response to different stimulus intensities in 2-month-old SOD2$^{+/-}$ mice, and an even stronger decrease in 6-month-old SOD2$^{+/-}$ mice (Fig. 3Ba). We obtained similar results when we analyzed the NMDARs-dependent response. We observed a decrease in NMDARs-dependent synaptic response in 2-month-old SOD2$^{+/-}$ mice and a stronger decrease in 6-month-old SOD2$^{+/-}$ mice (Fig. 3Bb). Since we found a decrease in the NMDARs-dependent response by analysis of input-output curves in SOD2$^{+/-}$ mice (Fig. 3B) we decided to analyze if changes in the distribution of NMDA receptors in synaptic and extrasynaptic membranes could be contributing to the effect observed in SOD2$^{+/-}$ mice. Several reports demonstrate that tyrosine phosphorylation of the NMDARs GluN2B subunit is strongly associated with surface expression of this receptor. This surface expression of the receptors can be synaptic and extrasynaptic. For instance, phosphorylation on tyrosine 1472 determines the surface expression of NMDARs in the synaptic zone [24], and phosphorylated tyrosine 1336 is associated with enrichment of the receptor in extrasynaptic membranes [23]. We did not observe significant differences in the phosphorylated status of NMDARs in 2 and 6-month-old WT mice (Fig. 3Ca, Cc and Cd) or in the specific phosphorylation, that maintains NMDARs in the synaptic zone (p-1472), in 2 and 6-month-old SOD2$^{+/-}$ mice when compared with WT mice (Fig. 3Cb and Cc). However, the specific phosphorylation that enriches NMDARs in the extrasynaptic zone (p-1336) increased by approximately 60% in 2 and 6-month-old SOD2$^{+/-}$ mice (Fig. 3Cb and Cd), generating an imbalance between synaptic and extrasynaptic NMDARs (Fig. 3Ce). Consistent with the idea that an increment of certain types of oxidative stress may compromise cognitive functions and synaptic strength, we evaluated synaptic plasticity in WT and SOD2$^{+/-}$ mice of different ages by studying LTP magnitude in hippocampal CA3-CA1 transmission, which also correlates with memory and learning [48]. We used a weak HFS protocol (2 trains at 100 Hz for the LTP induction) and found that LTP induction is compromised in 6-month-old SOD2$^{+/-}$ mice when compared with same age WT animals (Fig. 3Da and Db). Nevertheless, 2-month-old SOD2$^{+/-}$ mice had the ability to induce LTP, which was maintained for at least 15 min (Fig. 3Da and Db). These results suggest that the accumulation of oxidative damage may induce pathological changes in the hippocampus and affect synaptic function, in part, due to an increase in the extrasynaptic NMDARs population.

3.4. NMDARs associated signaling is altered in SOD2$^{+/-}$ mice

Because of the increment in the extrasynaptic NMDARs population, detected by tyrosine 1336 phosphorylation, we analyzed three targets implicated in NMDARs signaling. These were CREB, STEP$_{61}$, and PTEN. Previous reports indicate that synaptic activity triggered by NMDARs activation induces CREB-dependent transcription. Phosphorylation of CREB on serine 133 is often regarded as a marker for CREB-mediated transcription [20,49], and extrasynaptic NMDARs can decrease CREB activation [50]. Therefore, we analyzed the levels of p-CREB (S133) in the hippocampus of 2 and 6-month-old WT and SOD2$^{+/-}$ mice by immunofluorescence (Fig. 4A). We found that 6-month-old SOD2$^{+/-}$ mice show a significant decrease of p-CREB in the CA3 region of the hippocampus (Fig. 4Aa and Ac), but not in the CA1 zone (Fig. 4Ab). Furthermore, we examined p-CREB levels by Western-blot analysis and we found a similar decrease in 6 month-old SOD2$^{+/-}$ mice (Supplementary Fig. 4B). On the other hand, we analyzed two phosphatases that are directly and indirectly implicated in the phosphorylated status of NMDARs: STEP$_{61}$ and PTEN [15]. STEP$_{61}$ regulates the phosphorylation state and surface density on NMDARs through two parallel pathways: the direct dephosphorylation of tyrosine 1472; or indirectly, through dephosphorylation and inactivation of Fyn [25,26]. Moreover, extrasynaptic NMDARs stimulation is associated with Calpain activation and STEP cleavage, which produces a degradation product of 33 kDa (STEP$_{33}$) [22,26]. The deregulation of this phosphatase has been implicated in several neurodegenerative disorders, most notably AD and HD [51,52]. We measured the levels of STEP by immunofluorescence (Fig. 4B) and immunoblot analysis (Fig. 4C). We found that the levels of STEP are increased in the CA1 region of SOD2$^{+/-}$ animals. Indeed, 2 and 6-month-old SOD2$^{+/-}$ mice show a 1.5–2-fold increment with respect to WT mice (Fig. 4Ba and Bb). In the CA3 region, we found a significant increase of STEP levels in 6-month-old SOD2$^{+/-}$ mice when compared with 6-month-old WT and 2-month-old SOD2$^{+/-}$ mice (Fig. 4Ba and Bc). A similar increase in STEP levels was reported for transgenic mice models of AD and HD [52,53]. Immunoblot analysis showed two isoforms of STEP present in the hippocampus, STEP$_{61}$, and STEP$_{33}$ (Fig. 4C). STEP$_{61}$ is the active form of this phosphatase and STEP$_{33}$ is a degradation product associated to Calpain activation when extrasynaptic NMDARs are activated [22,26]. There are no significant differences in STEP$_{61}$ and STEP$_{33}$ levels between the WT mice experimental groups (Fig. 4Ca and Cc). In this case, the band corresponding to STEP$_{33}$ is very weak. In 2-month-old SOD2$^{+/-}$ mice, the levels of the two STEP isoforms are similar to those of 2 and 6-month-old WT animals. On the other hand, we detected an increase of STEP$_{61}$ and a strong increase in STEP$_{33}$ in 6-month-old SOD2$^{+/-}$ mice (Fig. 4Cb and Cc). We also evaluated PTEN by immunoblot analysis (Fig. 4C). This phosphatase has also been implicated in several neuropathologies such as AD and Stroke through a similar mechanism dependent on the phosphorylation status of NMDARs [30,32,33]. Significant differences were observed between 2 and 6-month-old WT mice possibly due to normal aging (Fig. 4Ca and Cc). Additionally, we found a 50% PTEN increase in 6-month-old SOD2$^{+/-}$ mice compared with same age WT mice (Fig. 4Cb). These results indicate that oxidative stress accumulation in the hippocampus alters signaling mediated by activation of NMDARs, in this case through a decrease in CREB activation. This activation is also inhibited by extrasynaptic-NMDARs activation. Furthermore, we found an increase of two phosphatases implicated in the phosphorylation state and localization of NMDARs that are involved in several neuropathologies.

4. Discussion

Using a heterozygous knockout mouse model (SOD2$^{+/-}$) with compromised antioxidant capacity, we showed that oxidative conditions affect signaling associated with the distribution of NMDARs, which trigger hippocampal-dependent functional and behavioral

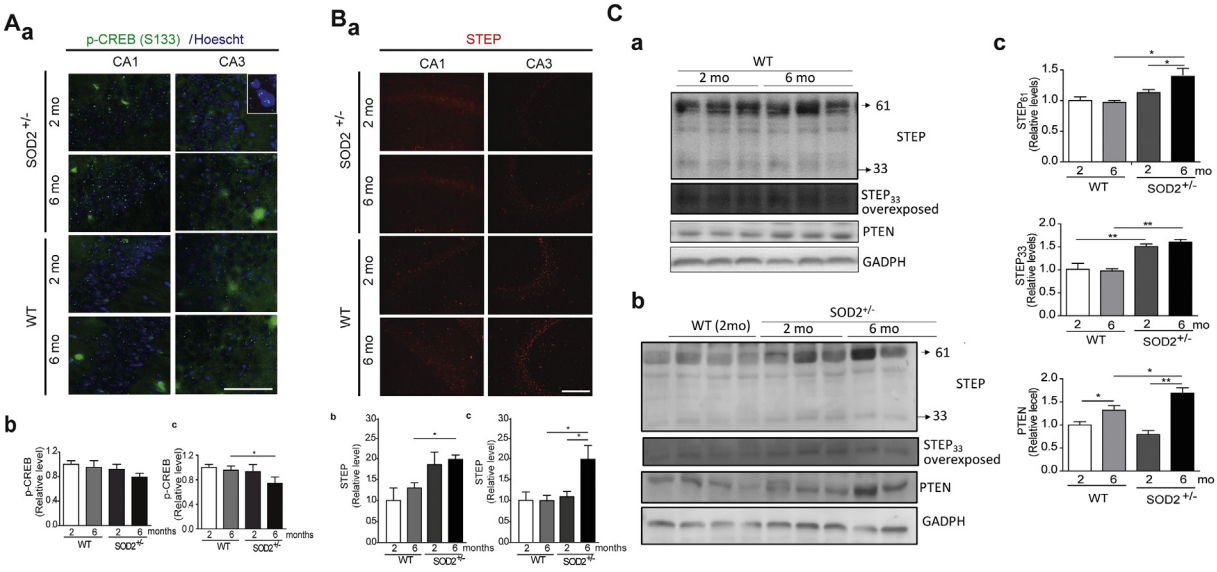

Fig. 4. NMDARs associated signaling is altered in SOD2$^{+/-}$. Aa. Representative immunofluorescence images of p-CREB (S133) in the CA1 and CA3 hippocampal regions from 2 and 6-month-old WT and SOD2$^{+/-}$ mice. The graphs show relative levels of p-CREB in the CA1 (Ab) and CA3 (Ac) regions. The inset shows p-CREB staining in the nucleus. Ba. Representative immunofluorescence images of STEP in CA1 and CA3 hippocampal regions from 2 and 6-month-old WT and SOD2$^{+/-}$ mice. Bb. The graphs show quantification of fluorescence intensity in the CA1. Bc. The graphs show quantification of fluorescence intensity in the CA3 region. C. Immunoblot of $STEP_{61}$, $STEP_{33}$ and PTEN from hippocampi lysates from 2 and 6-month-old WT and SOD2$^{+/-}$ mice (Ca and Cb, respectively). Cc. Densitometric analysis of $STEP_{61}$, $STEP_{33,}$ and PTEN in hippocampi lysates from 2-month-old WT mice and 6 and 2 and 6-month-old SOD2$^{+/-}$ mice. Bar = 100 μm. Three animals were used per experimental group for immunofluorescence analyses and six animals for biochemical assays. Data are means ± S.E. Statistical differences were calculated by ANOVA, followed by post hoc Bonferroni's test. Asterisks indicate statistical significance of the observed differences (*$p < 0.05$; **$p < 0.01$).

consequences. In general, there are two mechanisms through which ROS affect ion channels: 1) by direct oxidation of the receptors' amino acid residues or 2) by interfering with signaling pathways that regulate the channels [12]. NMDARs activity can be regulated by hydroxyl radicals directly on redox modulatory sites [54–56]. However, these receptors are not the only channels that are affected by ROS in hippocampal-dependent processes such as learning and memory. The Ryanodine receptors (RyRs) are a family of Ca^{2+} release channels found in intracellular Ca^{2+} storage organelles. Dysfunction of these redox-sensitive channels affects the capacity of neural circuits to generate LTP [57]. In this work, we focused on how oxidative damage alters the signaling implicated in the distribution of NMDARs. Our experiments on hippocampal slices from SOD2$^{+/-}$ animals, which have a 79% decrease in SOD2 activity in the brain [41], show that oxidative stress affects synaptic connectivity mediated by NMDARs. Given the importance of NMDARs in synaptic transmission [15,58], the regulation of their downstream signaling by oxidative stress provides a mechanism for synaptic dysfunction in several neurological conditions where increased ROS levels are main regulators [59].

NMDARs are more dynamic than originally thought, and neurons are able to regulate the number, distribution and subunit composition of synaptic and extrasynaptic receptors [17,60,61]. However, the signals and mechanisms controlling the presence of NMDARs in different cellular domains are dependent on the phosphorylation state of the GluN2B-subunit [23]. Phosphorylation on tyrosine 1472 of GluN2B is critical for maintaining the synaptic form of NMDARs and preventing their endocytosis. On the other hand, phosphorylation of GluN2B on tyrosine 1336 is associated with the enrichment of extrasynaptic NMDARs [23]. Both phosphorylation sites are substrates for the Src-family kinase Fyn [24]. Moreover, the phosphorylation state of NMDARs is modulated by STEP through two parallel pathways: by direct dephosphorylation of GluN2B-Tyr 1472 [23,62], and indirectly via dephosphorylation and inactivation of Fyn [63]. On the other hand, STEP is differentially regulated by synaptic and extrasynaptic NMDARs [22]. Dephosphorylation of GluN2B-Tyr 1472 can also be performed by PTEN. This phosphatase is directly involved in NMDARs-dependent LTD [29,31] and has been implicated in the pathological mechanism of recurrent migraine through dephosphorylation of tyrosine 1472 in a rat model [64]. In addition, PTEN has also been associated with other neuropathologies such as AD and Stroke through similar mechanisms dependent on the phosphorylated status of NMDARs [30,32,33]. Moreover, considerable effort has been recently dedicated to understanding how STEP deregulation contributes to the pathophysiology of neuropsychiatric disorders such as AD, HD, and schizophrenia [51,52,65].

NMDARs are localized in distinct compartments in the neuronal membrane where they initiate signaling pathways when activated by glutamate [66,67]. Activation of synaptic NMDARs is coupled with the activation of ERK and is involved in synaptic strengthening and neuronal survival [50]. Moreover, a previous report indicates that Cdk5 regulation of GluN2B enhances memory in a rat model [68]. Activated ERK phosphorylates several synaptic and cytoplasmic proteins and is translocated to the nucleus where it phosphorylates and activates transcription factors such as CREB and Elk-1, which are involved in dendritic spine remodeling [20,69]. In contrast, extrasynaptic NMDAR activation is linked to the activation of p38 and cell death pathways [22]. When synaptic NMDARs are stimulated, $STEP_{61}$ is ubiquitinated and eliminated from synaptic sites via rapid degradation through the ubiquitin-proteasome system. On the other hand, diminished NMDARs-dependent synaptic response contributes to increased STEP levels at synaptic sites [22].

Using a combination of biochemical, histological, electrophysiological and behavioral tools we identified NMDARs downstream signaling mediated by the receptors´ synaptic and extrasynaptic localization. We show that the deleterious effects induced by a mechanism that includes oxidative stress are regulated by the distribution of NMDARs. We found increased levels of oxidative stress markers in 6-month-old WT mice, which can be considered as normal aging. In SOD2$^{+/-}$ mice, with reduced antioxidant capacity, oxidative stress markers are increased in 2 and 6-month-old mice. However, cognitive performance failure is only observed in 6-month-old animals, suggesting that the effects mediated by ROS need longer exposure times.

Moreover, the alterations in synaptic transmission, mainly those related with the response of synaptic-NMDARs present in 2 and 6-old-month heterozygous knockout mice can be induced by an increase in the extrasynaptic-NMDARs population (measured by p-1336 GluN2B levels). The increase in this population can be triggered by higher STEP [70] and PTEN [71] levels as a result of proteasome system inactivation and the consequent inhibition of protein degradation. This situation may contribute to the decrease in the synaptic form of NMDARs. STEP degradation is required for sustained ERK activation. The activation of these phosphatases induces decreased levels of the ERK target p-CREB, reducing survival signaling in neurons. We only found alterations in CREB signaling in 6-month-old $SOD2^{+/-}$ mice, effectively demonstrating alterations in NMDARs downstream signaling. Several neuropathologies in which dysfunction of NMDARs has been implicated, including AD [3], PD [2] and HD [45], have also been associated with deregulation of the neuron's oxidative status, suggesting that such a common event as oxidative stress can affect synaptic maintenance and function. The role of oxidative status in the control of NMDARs distribution and downstream signaling offers a mechanism that provides a better understanding of neuropathologies in which glutamatergic synaptic transmission is compromised.

The mechanism described above is the main contributor of alterations in intracellular signaling. Crosstalk at the ERK level points to other upstream molecules, signaling for events associated with similar brain functions, able to impact on cellular performance. The potassium channel KCNB1 (Kv2.1) in its oxidized form causes cellular alterations and behavioral deficits in a mouse model of traumatic brain injury [72]. The contribution of Src tyrosine kinases was demonstrated using the inhibitor Disatinib [72]. Crosstalk between Src kinase and ERK has been demonstrated in an ischemia model [73]. Src is upstream of ERK signaling and controls its activation through protein phosphatase 2A [73]. As described above, ERK controls CREB phosphorylation. The regulation of the CREB master transcription factor is widely associated with behavioral processes and is decreased in chronic and acute pathologies related to neuronal plasticity dysfunction [20,74]. KCNB1 contributes to increased excitability in hippocampal neurons in an AD mouse model [75]. Therefore, is possible to associate acute and chronic pathological conditions to modifications in potassium channels. Oxidized forms of these channels allow placing this mechanism as an important contributor to cellular dysfunction in different tissues including vasculature [76,77], skeletal muscle [78,79] and brain [80,81]. NMDAR and KCNB1 signaling are emerging as important participants in the mechanisms of synaptic plasticity and neurodegeneration in association with the cell's oxidative status. We focused on three effectors of NMDAR signaling (PTEN, STEP, and p-CREB), which are possible targets for intervention. The activation of NMDAR signaling is dependent on whether the receptors are localized in the synapse or in extrasynaptic areas.

Neurons are particularly sensitive to oxidative stress [12] because, in general, they are unable of divide [82]. For that reason, the battery of antioxidant mechanisms is wide and diverse [83], and hypofunction of any of these components could be potentially catastrophic for neurons. For example, in the neuropathological conditions we have mentioned, in addition to oxidative stress and synaptic failure, there are alterations of the ubiquitin-proteasome system [84,85]; STEP dysregulation [25,26,51,52]; and alterations in CREB dependent signaling [86], bioenergetics and mitochondrial function [87,88].

Understanding how glutamate receptors are regulated under oxidative stress conditions provides the bases for understanding the regulation of processes such as synapse formation, learning and memory, and neuropathologies; opening opportunities for the development of treatments for diseases in which the distribution and signaling of NMDARs are compromised.

Supplementary data to this article can be found online at https://doi.org/10.1016/j.bbadis.2018.03.019.

Transparency document

The http://dx.doi.org/10.1016/j.bbadis.2018.03.019 associated this article can be found, in online version.

Acknowledgments

This work has been supported by grants FONDECYT N° 11121206, Research Team Project in Science and Technology (ACT1411), Basal Center for Excellence in Science and Technology (AFB 170005, PFB 12/2007), Sociedad Química y Minera de Chile (SQM) for special grant "The role of lithium in human health and disease" and BMBF 20150065 (PCI) to WC, by a pre-doctoral fellowship from CONICYT to FJC (21161392), FONDECYT N° 11171155 and Inicio 2016 of Vicerrectoría de Investigación, Pontificia Universidad Católica de Chile to MR.

Conflict to interest

The authors declare that they have no competing interests.

Author contributions

FJC and WC conceived the project and designed the experiments. FJC, AM and WC wrote the manuscript. FJC performed most of the experiments and analyzed the data. RGM performed some experiments and analyzed the data. WC supervised the study. AM & MR edited the final version.

References

[1] T.I. Williams, B.C. Lynn, W.R. Markesbery, M.A. Lovell, Increased levels of 4-hydroxynonenal and acrolein, neurotoxic markers of lipid peroxidation, in the brain in mild cognitive impairment and early Alzheimer's disease, Neurobiol. Aging 27 (2006) 1094–1099.
[2] G.H. Kim, J.E. Kim, S.J. Rhie, S. Yoon, The role of oxidative stress in neurodegenerative diseases, Exp. Neurobiol. 24 (2015) 325–340.
[3] R. von Bernhardi, J. Eugenin, Alzheimer's disease: redox dysregulation as a common denominator for diverse pathogenic mechanisms, Antioxid. Redox Signal. 16 (2012) 974–1031.
[4] J.J. Perry, A.S. Hearn, D.E. Cabelli, H.S. Nick, J.A. Tainer, D.N. Silverman, Contribution of human manganese superoxide dismutase tyrosine 34 to structure and catalysis, Biochemistry 48 (2009) 3417–3424.
[5] E.K. Pias, O.Y. Ekshyyan, C.A. Rhoads, J. Fuseler, L. Harrison, T.Y. Aw, Differential effects of superoxide dismutase isoform expression on hydroperoxide-induced apoptosis in PC-12 cells, J. Biol. Chem. 278 (2003) 13294–13301.
[6] H.B. Kwak, Y. Lee, J.H. Kim, H. Van Remmen, A.G. Richardson, J.M. Lawler, MnSOD overexpression reduces fibrosis and pro-apoptotic signaling in the aging mouse heart, J. Gerontol. A Biol. Sci. Med. Sci. 70 (2015) 533–544.
[7] A. Hosoki, S. Yonekura, Q.L. Zhao, Z.L. Wei, I. Takasaki, Y. Tabuchi, L.L. Wang, S. Hasuike, T. Nomura, A. Tachibana, K. Hashiguchi, S. Yonei, T. Kondo, Q.M. Zhang-Akiyama, Mitochondria-targeted superoxide dismutase (SOD2) regulates radiation resistance and radiation stress response in HeLa cells, J. Radiat. Res. 53 (2012) 58–71.
[8] Y. Ishihara, T. Takemoto, K. Itoh, A. Ishida, T. Yamazaki, Dual role of superoxide dismutase 2 induced in activated microglia: oxidative stress tolerance and convergence of inflammatory responses, J. Biol. Chem. 290 (2015) 22805–22817.
[9] P. Becuwe, M. Ennen, R. Klotz, C. Barbieux, S. Grandemange, Manganese superoxide dismutase in breast cancer: from molecular mechanisms of gene regulation to biological and clinical significance, Free Radic. Biol. Med. 77 (2014) 139–151.
[10] K.A. Jellinger, Basic mechanisms of neurodegeneration: a critical update, J. Cell. Mol. Med. 14 (2010) 457–487.
[11] D. Beracochea, A. Krazem, N. Henkouss, G. Haccard, M. Roller, E. Fromentin, Intake of wild blueberry powder improves episodic-like and working memory during normal aging in mice, Planta Med. 82 (2016) 1163–1168.
[12] R. Patel, F. Sesti, Oxidation of ion channels in the aging nervous system, Brain Res. 1639 (2016) 174–185.
[13] S. Cull-Candy, S. Brickley, M. Farrant, NMDA receptor subunits: diversity, development and disease, Curr. Opin. Neurobiol. 11 (2001) 327–335.
[14] A. Barria, R. Malinow, NMDA receptor subunit composition controls synaptic plasticity by regulating binding to CaMKII, Neuron 48 (2005) 289–301.
[15] C.G. Lau, R.S. Zukin, NMDA receptor trafficking in synaptic plasticity and neuropsychiatric disorders, Nat. Rev. Neurosci. 8 (2007) 413–426.
[16] R.E. Sirrieh, D.M. MacLean, V. Jayaraman, A conserved structural mechanism of NMDA receptor inhibition: a comparison of ifenprodil and zinc, J. Gen. Physiol. 146 (2015) 173–181.
[17] G.E. Hardingham, H. Bading, Synaptic versus extrasynaptic NMDA receptor

signalling: implications for neurodegenerative disorders, Nat. Rev. Neurosci. 11 (2010) 682–696.
[18] L.J. Chandler, G. Sutton, N.R. Dorairaj, D. Norwood, N-methyl D-aspartate receptor-mediated bidirectional control of extracellular signal-regulated kinase activity in cortical neuronal cultures, J. Biol. Chem. 276 (2001) 2627–2636.
[19] S. Papadia, P. Stevenson, N.R. Hardingham, H. Bading, G.E. Hardingham, Nuclear Ca^{2+} and the cAMP response element-binding protein family mediate a late phase of activity-dependent neuroprotection, J. Neurosci. 25 (2005) 4279–4287.
[20] G.E. Hardingham, F.J. Arnold, H. Bading, Nuclear calcium signaling controls CREB-mediated gene expression triggered by synaptic activity, Nat. Neurosci. 4 (2001) 261–267.
[21] G.E. Hardingham, Y. Fukunaga, H. Bading, Extrasynaptic NMDARs oppose synaptic NMDARs by triggering CREB shut-off and cell death pathways, Nat. Neurosci. 5 (2002) 405–414.
[22] J. Xu, P. Kurup, Y. Zhang, S.M. Goebel-Goody, P.H. Wu, A.H. Hawasli, M.L. Baum, J.A. Bibb, P.J. Lombroso, Extrasynaptic NMDA receptors couple preferentially to excitotoxicity via calpain-mediated cleavage of STEP, J. Neurosci. 29 (2009) 9330–9343.
[23] S.M. Goebel-Goody, K.D. Davies, R.M. Alvestad Linger, R.K. Freund, M.D. Browning, Phospho-regulation of synaptic and extrasynaptic N-methyl-D-aspartate receptors in adult hippocampal slices, Neuroscience 158 (2009) 1446–1459.
[24] F. Xu, M.R. Plummer, G.W. Len, T. Nakazawa, T. Yamamoto, I.B. Black, K. Wu, Brain-derived neurotrophic factor rapidly increases NMDA receptor channel activity through Fyn-mediated phosphorylation, Brain Res. 1121 (2006) 22–34.
[25] E.M. Snyder, Y. Nong, C.G. Almeida, S. Paul, T. Moran, E.Y. Choi, A.C. Nairn, M.W. Salter, P.J. Lombroso, G.K. Gouras, P. Greengard, Regulation of NMDA receptor trafficking by amyloid-beta, Nat. Neurosci. 8 (2005) 1051–1058.
[26] S.M. Goebel-Goody, M. Baum, C.D. Paspalas, S.M. Fernandez, N.C. Carty, P. Kurup, P.J. Lombroso, Therapeutic implications for striatal-enriched protein tyrosine phosphatase (STEP) in neuropsychiatric disorders, Pharmacol. Rev. 64 (2012) 65–87.
[27] T.H. Nguyen, J. Liu, P.J. Lombroso, Striatal enriched phosphatase 61 dephosphorylates Fyn at phosphotyrosine 420, J. Biol. Chem. 277 (2002) 24274–24279.
[28] N. Chang, Y.H. El-Hayek, E. Gomez, Q. Wan, Phosphatase PTEN in neuronal injury and brain disorders, Trends Neurosci. 30 (2007) 581–586.
[29] K.L. Arendt, M. Benoist, A. Lario, J.E. Draffin, M. Munoz, J.A. Esteban, PTEN counteracts PIP3 upregulation in spines during NMDA-receptor-dependent long-term depression, J. Cell Sci. 127 (2014) 5253–5260.
[30] S. Knafo, J.A. Esteban, PTEN: local and global modulation of neuronal function in health and disease, Trends Neurosci. 40 (2017) 83–91.
[31] S. Jurado, M. Benoist, A. Lario, S. Knafo, C.N. Petrok, J.A. Esteban, PTEN is recruited to the postsynaptic terminal for NMDA receptor-dependent long-term depression, EMBO J. 29 (2010) 2827–2840.
[32] S. Zhang, C. Taghibiglou, K. Girling, Z. Dong, S.Z. Lin, W. Lee, W.C. Shyu, Y.T. Wang, Critical role of increased PTEN nuclear translocation in excitotoxic and ischemic neuronal injuries, J. Neurosci. 33 (2013) 7997–8008.
[33] S. Knafo, C. Sanchez-Puelles, E. Palomer, I. Delgado, J.E. Draffin, J. Mingo, T. Wahle, K. Kaleka, L. Mou, I. Pereda-Perez, E. Klosi, E.B. Faber, H.M. Chapman, L. Lozano-Montes, A. Ortega-Molina, L. Ordonez-Gutierrez, F. Wandosell, J. Vina, C.G. Dotti, R.A. Hall, R. Pulido, N.Z. Gerges, A.M. Chan, M.R. Spaller, M. Serrano, C. Venero, J.A. Esteban, PTEN recruitment controls synaptic and cognitive function in Alzheimer's models, Nat. Neurosci. 19 (2016) 443–453.
[34] W.W. Anderson, G.L. Collingridge, Capabilities of the WinLTP data acquisition program extending beyond basic LTP experimental functions, J. Neurosci. Methods 162 (2007) 346–356.
[35] M. Chen, T.J. Lu, X.J. Chen, Y. Zhou, Q. Chen, X.Y. Feng, L. Xu, W.H. Duan, Z.Q. Xiong, Differential roles of NMDA receptor subtypes in ischemic neuronal cell death and ischemic tolerance, Stroke 39 (2008) 3042–3048.
[36] R. Morris, Developments of a water-maze procedure for studying spatial learning in the rat, J. Neurosci. Methods 11 (1984) 47–60.
[37] C.V. Vorhees, M.T. Williams, Morris water maze: procedures for assessing spatial and related forms of learning and memory, Nat. Protoc. 1 (2006) 848–858.
[38] F.G. Serrano, C. Tapia-Rojas, F.J. Carvajal, J. Hancke, W. Cerpa, N.C. Inestrosa, Andrographolide reduces cognitive impairment in young and mature AbetaPPswe/PS-1 mice, Mol. Neurodegener. 9 (2014) 61.
[39] F.J. Carvajal, J.M. Zolezzi, C. Tapia-Rojas, J.A. Godoy, N.C. Inestrosa, Tetrahydrohyperforin decreases cholinergic markers associated with amyloid-beta plaques, 4-hydroxynonenal formation, and caspase-3 activation in AbetaPP/PS1 mice, J. Alzheimers Dis. 36 (2013) 99–118.
[40] F.G. Serrano, C. Tapia-Rojas, F.J. Carvajal, J. Hancke, W. Cerpa, N.C. Inestrosa, Andrographolide reduces cognitive impairment in young and mature AbetaPPswe/PS-1 mice, Mol. Neurodegener. 9 (2014) 61.
[41] H. Van Remmen, C. Salvador, H. Yang, T.T. Huang, C.J. Epstein, A. Richardson, Characterization of the antioxidant status of the heterozygous manganese superoxide dismutase knockout mouse, Arch. Biochem. Biophys. 363 (1999) 91–97.
[42] R.F. Langston, C.H. Stevenson, C.L. Wilson, I. Saunders, E.R. Wood, The role of hippocampal subregions in memory for stimulus associations, Behav. Brain Res. 215 (2010) 275–291.
[43] C. Ji, V. Amarnath, J.A. Pietenpol, L.J. Marnett, 4-hydroxynonenal induces apoptosis via caspase-3 activation and cytochrome c release, Chem. Res. Toxicol. 14 (2001) 1090–1096.
[44] Q.G. Zhang, M.D. Laird, D. Han, K. Nguyen, E. Scott, Y. Dong, K.M. Dhandapani, D.W. Brann, Critical role of NADPH oxidase in neuronal oxidative damage and microglia activation following traumatic brain injury, PLoS One 7 (2012) e34504.
[45] J. Gil-Mohapel, P.S. Brocardo, B.R. Christie, The role of oxidative stress in Huntington's disease: are antioxidants good therapeutic candidates? Curr. Drug Targets 15 (2014) 454–468.
[46] S.P. Brooks, N. Janghra, G.V. Higgs, Z. Bayram-Weston, A. Heuer, L. Jones, S.B. Dunnett, Selective cognitive impairment in the YAC128 Huntington's disease mouse, Brain Res. Bull. 88 (2012) 121–129.
[47] X. Zhou, W. da Li, B.L. Yuan, L.J. Niu, X.Y. Yang, Z.B. Zhou, X.H. Chen, X. Feng, Lithium treatment prevents apoptosis in neonatal rat Hippocampus resulting from sevoflurane exposure, Neurochem. Res. 41 (2016) 1993–2005.
[48] J.R. Whitlock, A.J. Heynen, M.G. Shuler, M.F. Bear, Learning induces long-term potentiation in the hippocampus, Science 313 (2006) 1093–1097.
[49] Y.H. Huang, Y. Lin, T.E. Brown, M.H. Han, D.B. Saal, R.L. Neve, R.S. Zukin, B.A. Sorg, E.J. Nestler, R.C. Malenka, Y. Dong, CREB modulates the functional output of nucleus accumbens neurons: a critical role of N-methyl-D-aspartate glutamate receptor (NMDAR) receptors, J. Biol. Chem. 283 (2008) 2751–2760.
[50] G.E. Hardingham, H. Bading, Coupling of extrasynaptic NMDA receptors to a CREB shut-off pathway is developmentally regulated, Biochim. Biophys. Acta 1600 (2002) 148–153.
[51] J. Xu, M. Chatterjee, T.D. Baguley, J. Brouillette, P. Kurup, D. Ghosh, J. Kanyo, Y. Zhang, K. Seyb, C. Ononenyi, E. Foscue, G.M. Anderson, J. Gresack, G.D. Cuny, M.A. Glicksman, P. Greengard, T.T. Lam, L. Tautz, A.C. Nairn, J.A. Ellman, P.J. Lombroso, Inhibitor of the tyrosine phosphatase STEP reverses cognitive deficits in a mouse model of Alzheimer's disease, PLoS Biol. 12 (2014) e1001923.
[52] C.M. Gladding, M.D. Sepers, J. Xu, L.Y. Zhang, A.J. Milnerwood, P.J. Lombroso, L.A. Raymond, Calpain and STriatal-enriched protein tyrosine phosphatase (STEP) activation contribute to extrasynaptic NMDA receptor localization in a Huntington's disease mouse model, Hum. Mol. Genet. 21 (2012) 3739–3752.
[53] P. Kurup, Y. Zhang, J. Xu, D.V. Venkitaramani, V. Haroutunian, P. Greengard, A.C. Nairn, P.J. Lombroso, Abeta-mediated NMDA receptor endocytosis in Alzheimer's disease involves ubiquitination of the tyrosine phosphatase STEP61, J. Neurosci. 30 (2010) 5948–5957.
[54] E. Aizenman, K.A. Hartnett, I.J. Reynolds, Oxygen free radicals regulate NMDA receptor function via a redox modulatory site, Neuron 5 (1990) 841–846.
[55] E. Aizenman, S.A. Lipton, R.H. Loring, Selective modulation of NMDA responses by reduction and oxidation, Neuron 2 (1989) 1257–1263.
[56] E. Aizenman, Modulation of N-methyl-D-aspartate receptors by hydroxyl radicals in rat cortical neurons in vitro, Neurosci. Lett. 189 (1995) 57–59.
[57] A.C. Paula-Lima, T. Adasme, C. Hidalgo, Contribution of Ca^{2+} release channels to hippocampal synaptic plasticity and spatial memory: potential redox modulation, Antioxid. Redox Signal. 21 (2014) 892–914.
[58] P. Paoletti, C. Bellone, Q. Zhou, NMDA receptor subunit diversity: impact on receptor properties, synaptic plasticity and disease, Nat. Rev. Neurosci. 14 (2013) 383–400.
[59] S. Cahill-Smith, J.M. Li, Oxidative stress, redox signalling and endothelial dysfunction in ageing-related neurodegenerative diseases: a role of NADPH oxidase 2, Br. J. Clin. Pharmacol. 78 (2014) 441–453.
[60] A. Barria, R. Malinow, Subunit-specific NMDA receptor trafficking to synapses, Neuron 35 (2002) 345–353.
[61] L. Groc, M. Heine, S.L. Cousins, F.A. Stephenson, B. Lounis, L. Cognet, D. Choquet, NMDA receptor surface mobility depends on NR2A-2B subunits, Proc. Natl. Acad. Sci. U. S. A. 103 (2006) 18769–18774.
[62] K.W. Roche, S. Standley, J. McCallum, C. Dune Ly, M.D. Ehlers, R.J. Wenthold, Molecular determinants of NMDA receptor internalization, Nat. Neurosci. 4 (2001) 794–802.
[63] T.H. Nguyen, J. Liu, P.J. Lombroso, Striatal enriched phosphatase 61 dephosphorylates Fyn at phosphotyrosine 420, J. Biol. Chem. 277 (2002) 24274–24279.
[64] G. Qin, J. Xie, L. Chen, B. Wu, B. Gui, J. Zhou, PTEN inhibition preserves trigeminal nucleus caudalis neuron activation through tyrosine phosphorylation of the NR2B subunit at Tyr1472 of the NMDA receptor in a rat model of recurrent migraine, Neurol. Res. 38 (2016) 320–326.
[65] N.C. Carty, J. Xu, P. Kurup, J. Brouillette, S.M. Goebel-Goody, D.R. Austin, P. Yuan, G. Chen, P.R. Correa, V. Haroutunian, C. Pittenger, P.J. Lombroso, The tyrosine phosphatase STEP: implications in schizophrenia and the molecular mechanism underlying antipsychotic medications, Transl. Psychiatry 2 (2012) e137.
[66] G.E. Hardingham, F.J. Arnold, H. Bading, A calcium microdomain near NMDA receptors: on switch for ERK-dependent synapse-to-nucleus communication, Nat. Neurosci. 4 (2001) 565–566.
[67] A. Ivanov, C. Pellegrino, S. Rama, I. Dumalska, Y. Salyha, Y. Ben-Ari, I. Medina, Opposing role of synaptic and extrasynaptic NMDA receptors in regulation of the extracellular signal-regulated kinases (ERK) activity in cultured rat hippocampal neurons, J. Physiol. 572 (2006) 789–798.
[68] F. Plattner, A. Hernandez, T.M. Kistler, K. Pozo, P. Zhong, E.Y. Yuen, C. Tan, A.H. Hawasli, S.F. Cooke, A. Nishi, A. Guo, T. Wiederhold, Z. Yan, J.A. Bibb, Memory enhancement by targeting Cdk5 regulation of NR2B, Neuron 81 (2014) 1070–1083.
[69] E. Thiels, E. Klann, Extracellular signal-regulated kinase, synaptic plasticity, and memory, Rev. Neurosci. 12 (2001) 327–345.
[70] C.J. Fitzpatrick, P.J. Lombroso, The role of striatal-enriched protein tyrosine phosphatase (STEP) in cognition, Front. Neuroanat. 5 (2011) 47.
[71] R. Errafiy, C. Aguado, G. Ghislat, J.M. Esteve, A. Gil, M. Loutfi, E. Knecht, PTEN increases autophagy and inhibits the ubiquitin-proteasome pathway in glioma cells independently of its lipid phosphatase activity, PLoS One 8 (2013) e83318.
[72] W. Yu, R. Parakramaweera, S. Teng, M. Gowda, Y. Sharad, S. Thakker-Varia, J. Alder, F. Sesti, Oxidation of KCNB1 potassium channels causes neurotoxicity and cognitive impairment in a mouse model of traumatic brain injury, J. Neurosci. 36 (2016) 11084–11096.
[73] X. Hu, X. Wu, J. Xu, J. Zhou, X. Han, J. Guo, Src kinase up-regulates the ERK cascade through inactivation of protein phosphatase 2A following cerebral

ischemia, BMC Neurosci. 10 (2009) 74.
[74] C.A. Saura, J. Valero, The role of CREB signaling in Alzheimer's disease and other cognitive disorders, Rev. Neurosci. 22 (2011) 153–169.
[75] V. Frazzini, S. Guarnieri, M. Bomba, R. Navarra, C. Morabito, M.A. Mariggio, S.L. Sensi, Altered Kv2.1 functioning promotes increased excitability in hippocampal neurons of an Alzheimer's disease mouse model, Cell Death Dis. 7 (2016) e2100.
[76] E.J. Behringer, R.L. Shaw, E.B. Westcott, M.J. Socha, S.S. Segal, Aging impairs electrical conduction along endothelium of resistance arteries through enhanced Ca^{2+}-activated K^+ channel activation, Arterioscler. Thromb. Vasc. Biol. 33 (2013) 1892–1901.
[77] A. Feher, Z. Broskova, Z. Bagi, Age-related impairment of conducted dilation in human coronary arterioles, Am. J. Physiol. Heart Circ. Physiol. 306 (2014) H1595–1601.
[78] D. Tricarico, R. Petruzzi, D.C. Camerino, Changes of the biophysical properties of calcium-activated potassium channels of rat skeletal muscle fibres during aging, Pflugers Arch. 434 (1997) 822–829.
[79] C. Vergara, B.U. Ramirez, Age-dependent expression of the apamin-sensitive calcium-activated K^+ channel in fast and slow rat skeletal muscle, Exp. Neurol. 146 (1997) 282–285.
[80] S. Farajnia, J.H. Meijer, S. Michel, Age-related changes in large-conductance calcium-activated potassium channels in mammalian circadian clock neurons, Neurobiol. Aging 36 (2015) 2176–2183.
[81] J.M. Power, W.W. Wu, E. Sametsky, M.M. Oh, J.F. Disterhoft, Age-related enhancement of the slow outward calcium-activated potassium current in hippocampal CA1 pyramidal neurons in vitro, J. Neurosci. 22 (2002) 7234–7243.
[82] K. Herrup, Y. Yang, Cell cycle regulation in the postmitotic neuron: oxymoron or new biology? Nat. Rev. Neurosci. 8 (2007) 368–378.
[83] J. Lewerenz, P. Maher, Control of redox state and redox signaling by neural antioxidant systems, Antioxid. Redox Signal. 14 (2011) 1449–1465.
[84] A.N. Hegde, The ubiquitin-proteasome pathway and synaptic plasticity, Learn. Mem. 17 (2010) 314–327.
[85] A.N. Hegde, S.C. Upadhya, Role of ubiquitin-proteasome-mediated proteolysis in nervous system disease, Biochim. Biophys. Acta 1809 (2011) 128–140.
[86] A. Wang, J.A. Bibb, Is CREB the angry bird that releases memory in Alzheimer's? Neuropsychopharmacology 36 (2011) 2153–2154.
[87] S. Cardoso, R.M. Seica, P.I. Moreira, Mitochondria as a target for neuroprotection: implications for Alzheimer s disease, Expert. Rev. Neurother. 17 (2017) 77–91.
[88] S. Cardoso, C. Carvalho, R. Marinho, A. Simoes, C.M. Sena, P. Matafome, M.S. Santos, R.M. Seica, P.I. Moreira, Effects of methylglyoxal and pyridoxamine in rat brain mitochondria bioenergetics and oxidative status, J. Bioenerg. Biomembr. 46 (2014) 347–355.